Phase-sensitive amplifier link with distributed Raman amplification

Downloaded from: https://research.chalmers.se, 2026-04-05 10:42 UTC

Citation for the original published paper (version of record):
Eliasson, H., Vijayan, K., Foo, B. et al (2018). Phase-sensitive amplifier link with distributed Raman amplification. Optics Express, 26(16): 19854-19863. http://dx.doi.org/10.1364/OE.26.019854

N.B. When citing this work, cite the original published paper.

research.chalmers.se offers the possibility of retrieving research publications produced at Chalmers University of Technology. It covers all kind of research output: articles, dissertations, conference papers, reports etc. since 2004. research.chalmers.se is administrated and maintained by Chalmers Library

(article starts on next page)

Research Article | Vol. 26, No. 16 | 6 Aug 2018 | OPTICS EXPRESS 19854
Optics EXPRESS

Phase-sensitive amplifier link with distributed Raman amplification

HENRIK ELIASSON,[1] KOVENDHAN VIJAYAN,[1] BENJAMIN FOO,[1] SAMUEL L. I. OLSSON,[1,2] EGON ASTRA,[3] MAGNUS KARLSSON,[1] AND PETER A. ANDREKSON[1,*]

[1] *Photonics Laboratory, Department of Microtechnology and Nanoscience, Chalmers University of Technology, SE-412 96, Gothenburg, Sweden*
[2] *Now at: Nokia Bell Labs, 791 Holmdel Road, Holmdel, NJ 07733, USA*
[3] *Thomas Johann Seebeck Department of Electronics, Tallinn University of Technology, Tallinn, Estonia*
[*] *peter.andrekson@chalmers.se*

Abstract: We demonstrate long-haul transmission using a hybrid amplifier approach combining distributed Raman amplification and lumped phase-sensitive amplification. Aside from the well-known resulting SNR improvement, distributed Raman amplification is included in an effort to improve the nonlinearity mitigation capability of the phase-sensitive amplifiers. When changing from phase-insensitive operation to phase-sensitive operation in a link employing distributed Raman amplification, the transmission reach at BER = 10^{-3} is increased from 15 to 44 spans of length 81 km while simultaneously increasing the optimal launch power by 2 dB.

© 2018 Optical Society of America under the terms of the OSA Open Access Publishing Agreement

OCIS codes: (060.0060) Fiber optics and optical communications; (060.2320) Fiber optics amplifiers and oscillators; (060.4370) Nonlinear optics, fibers.

References and links

1. J. Cartledge, F. Guiomar, F. Kschischang, G. Liga, and M. Yankov, "Digital signal processing for fiber nonlinearities," Opt. Express **25**(3), 1916–1936 (2017).
2. R. A. Fisher, B. R. Suydam, and D. Yevick, "Optical phase conjugation for time-domain undoing of dispersive self-phase-modulation effects," Opt. Lett. **8**(12), 611–613 (1983).
3. H. Hu, R. M. Jopson, A. H. Gnauck, S. Randel, and S. Chandrasekhar, "Fiber nonlinearity mitigation of WDM-PDM QPSK/16-QAM signals using fiber-optic parametric amplifiers based multiple optical phase conjugations," Opt. Express **25**(3), 1618–1628 (2017).
4. T. Umeki, T. Kazama, A. Sano, K. Shibahara, K. Suzuki, M. Abe, H. Takenouchi, and Y. Miyamoto, "Simultaneous nonlinearity mitigation in 92 × 180-Gbit/s PDM-16QAM transmission over 3840 km using PPLN-based guard-band-less optical phase conjugation," Opt. Express **24**(15), 16945–16951 (2016).
5. A. Ellis, M. McCarthy, M. Al-Khateeb, and S. Sygletos, "Capacity limits of systems employing multiple optical phase conjugators," Opt. Express **23**(16), 20381–20393 (2015).
6. L. Li, P. G. Patki, Y. B. Kwon, V. Stelmakh, B. D. Campbell, M. Annamalai, T. I. Lakoba and M. Vasilyev, "All-optical regenerator of multi-channel signals," Nat. Commun. **8**(1), 884 (2017).
7. D. Rafique, "Fiber nonlinearity compensation: Commercial applications and complexity analysis," J. Lightw. Technol. **34**(2), 544–553 (2016).
8. P. Rosa, S. T. Le, G. Rizzelli, M. Tan, and J. Ania-Castañón, "Signal power asymmetry optimisation for optical phase conjugation using Raman amplification," Opt. Express **23**(25), 31772–31778 (2015).
9. R. Tang, J. Lasri, P. Devgan, V. Grigoryan, P. Kumar, and M. Vasilyev, "Gain characteristics of a frequency nondegenerate phase-sensitive fiber-optic parametric amplifier with phase self-stabilized input," Opt. Express **13**(26), 10483–10493 (2005).
10. S. L. I. Olsson, B. Corcoran, C. Lundström, T. Eriksson, M. Karlsson, and P. A. Andrekson, "Phase-sensitive amplified transmission links for improved sensitivity and nonlinearity tolerance," J. Lightw. Technol. **33**(3), 710–721 (2015).
11. S. L. I. Olsson, H. Eliasson, E. Astra, M. Karlsson, and P. A. Andrekson, "Long-haul optical transmission link using low-noise phase-sensitive amplifiers," Nat. Commun. 9, 2513 (2018).
12. X. Liu, A. R. Chraplyvy, P. J. Winzer, R. W. Tkach and S. Chandrasekhar, "Phase-conjugated twin waves for communication beyond the Kerr nonlinearity limit," Nat. Photon. **7**(7), 560–568 (2013).
13. Z. Tong, C. Lundström, P. A. Andrekson, C. J. McKinstrie, M. Karlsson, D. J. Blessing, and L. Grüner-Nielsen, "Towards ultrasensitive optical links enabled by low-noise phase-sensitive amplifiers," Nat. Photon. **5**(7), 430–436 (2011).

#323386 https://doi.org/10.1364/OE.26.019854
Journal © 2018 Received 31 May 2018; revised 27 Jun 2018; accepted 28 Jun 2018; published 24 Jul 2018

Optics EXPRESS

14. H. Eliasson, S. L. I. Olsson, M. Karlsson, and P. A. Andrekson, "Mitigation of nonlinear distortion in hybrid Raman/phase-sensitive amplifier links," Opt. Express **24**(2), 888–900 (2016).
15. H. Eliasson, S. L. I. Olsson, M. Karlsson and P. A. Andrekson, "Experimental investigation of nonlinearity mitigation properties of a hybrid distributed Raman/phase-sensitive amplifier link," in Optical Fiber Communication Conference (OFC), Los Angeles, USA, paper Th3J.4. (2017).
16. C. Lundström, R. Malik, L. Grüner-Nielsen, B. Corcoran, S. L. I. Olsson, M. Karlsson, and P. A. Andrekson, "Fiber optic parametric amplifier with 10-dB net gain without pump dithering," IEEE Photon. Technol. Lett. **25**(3), 234–237 (2013).
17. X. Liu, S. Chandrasekhar, P. Winzer, B. Maheux-L, G. Brochu, and F. Trepanier, "Efficient fiber nonlinearity mitigation in 50-GHz-DWDM transmission of 256-Gb/s PDM-16QAM signals by folded digital-back-propagation and channelized FBG-DCMs," in Optical Fiber Communication Conference (OFC), San Fransisco, USA, paper Tu3A.8. (2014).
18. G. Rizzelli, P. Rosa, P. Corredera, and J. Ania-Castañón, "Transmission span optimization in fiber systems with cavity and random distributed feedback ultralong Raman laser amplification," J. Lightw. Technol. **35**(22), 4967–4972 (2017).
19. J. C. Bouteiller, K. Brar and C. Headley, "Quasi-constant signal power transmission," in European Conference on Optical Communication (ECOC), Copenhagen, Denmark, paper S3.04 (2002).
20. M. Vasilyev, B. Szalabofka, S. Tsuda, J. M. Grochocinski and A. F. Evans, "Reduction of Raman MPI and noise figure in dispersion-managed fibre," Electron. Lett. **38**(6), 271–272 (2002).
21. M. Vasilyev, "Raman-assisted transmission: Toward ideal distributed amplification," in Optical Fiber Communication Conference (OFC), Atlanta, USA, paper WB1 (2003).
22. S. L. I. Olsson, B. Corcoran, C. Lundström, E. Tipsuwannakul, S. Sygletos, A. Ellis, Z. Tong, M. Karlsson, and P. A. Andrekson, "Injection locking-based pump recovery for phase-sensitive amplified links," Opt. Express **21**(12), 14512–14529 (2013).
23. R. J. Essiambre, P. Winzer, J. Bromage and C. H. Kim, "Design of bidirectionally pumped fiber amplifiers generating double Rayleigh backscattering," IEEE Photon. Technol. Lett. **14**(7), 914–916 (2002).

1. Introduction

The main limiting factors to the transmission distance or data throughput of modern coherent long-haul fiber-optic communication links are the nonlinear distortion in the single-mode fiber (SMF) due to the Kerr effect and amplified stimulated emission (ASE) noise from inline optical amplifiers. One way of extending the limits imposed by fiber nonlinearities is to actively reverse or undo the nonlinear distortion which is to a large part deterministic in nature. One approach for mitigating the negative impact of nonlinearities is to use digital methods like digital back-propagation (DBP), digital pre-compensation (DPC), perturbation based compensation or nonlinear Fourier transforms (NLFTs) [1]. One advantage of digital approaches, with the possible exception of NLFT, is that the transmission link itself does not have to be modified, limiting the increased complexity to the transceiver hardware. This makes digital approaches easier to implement in existing infrastructure. Another group of methods for mitigation of nonlinear distortion is all-optical approaches, relying on all-optical signal processing to compensate the nonlinear distortion. The most common all-optical approach is to use optical phase conjugation (OPC), placing one or more phase conjugation devices inline in a serial manner along the link [2–5]. An advantage of all-optical approaches is the potential to mitigate nonlinear distortion over large optical bandwidths or multiple channels [6] compared to digital approaches which are bandwidth-limited by the transceiver electrical bandwidth as well as computational complexity which can be prohibitively large already for compensation of one channel [7]. The span power map is an important parameter in optimizing the efficiency of the nonlinearity mitigation in OPC links and can be manipulated using distributed Raman amplification (DRA) [8]. Another all-optical approach for mitigation of nonlinear distortion is to use the copier-phase-sensitive amplifier (PSA) scheme [9]. In this scheme, a copier is used at the transmitter to generate a phase-conjugated copy (or idler) from the signal. Both waves are then transmitted and propagated in parallel followed by coherent superposition in the PSAs enabling nonlinearity mitigation [10, 11]. This scheme has many similarities to the phase-conjugated twin waves (PCTWs) concept where the signal and its phase-conjugated copy are transmitted on orthogonal polarization states followed by coherent superposition in receiver digital signal processing (DSP) [12]. Thus in the case of PCTW

Optics EXPRESS

periodic nonlinearity mitigation is not possible. An inherent disadvantage to both the copier-PSA and PCTW scheme is that 50 % spectral efficiency is sacrificed due to the co-propagation of a phase-conjugated copy alongside the signal. In addition to allowing for nonlinearity mitigation, the copier-PSA scheme also enables a 0 dB quantum-limited amplifier noise figure [13] compared to 3 dB for an Erbium-doped fiber amplifier (EDFA) or any other phase-insensitive amplifier (PIA).

A first-order perturbation analysis suggests that a flat or symmetric span power map in a PCTW link could lead to efficient nonlinearity mitigation [12]. This conclusion holds for copier-PSA links as well assuming that the signal and idler are separated in wavelength sufficiently for cross-phase modulation (XPM) to be negligible in comparison to self-phase modulation (SPM). Thus it is reasonable to believe that a flat or symmetric span power map could benefit the nonlinearity mitigation performance in PSA links in a similar manner as in OPC links [5]. We previously investigated this in simulations of a hybrid PSA-DRA link showing the potential for gains beyond what is predicted by the span noise figure (NF) improvement due to DRA [14]. Previously, we also reported on a small subset of the experimental results that we now will present [15].

In this paper, we present an experimental investigation of a hybrid approach where we combine DRA and PSAs. We provide experimental comparisons of 28 GBaud quadrature phase-shift keying (QPSK) long-haul transmission links using four different amplifier configurations. The investigated amplifier configurations are PIA, PSA, hybrid PIA-DRA and hybrid PSA-DRA. In [14] it was found that the impact of the span power map is larger at symbol rates where the dispersive length is on the order of, or shorter than the effective length which is why we use a 28 GBaud signal. In all cases we apply inline dispersion compensation since this is required in the PSA scenarios. For each of the amplifier configurations we optimize the ratio between dispersion pre- and post-compensation for maximizing the transmission reach in a nonlinear transmission regime. Using the optimal dispersion maps we then perform long-haul transmission experiments. When comparing the PIA-DRA case to the PSA-DRA case in long-haul transmission we observe a 2 dB increase in optimal launch power for the PSA-DRA case that is not present in the comparison between the PIA and the PSA case. We attribute this mainly to improved nonlinearity mitigation but also due to that the difference in equivalent span NF between the PIA-DRA and PSA-DRA case is smaller than the difference between the PIA and PSA case because of the noise contribution from DRA.

2. Experiment

A recirculating loop experiment was carried out to investigate if it is possible to improve the efficiency of the PSA nonlinearity compensation with the addition of DRA. The experimental setup is illustrated in Fig. 1. Light from a 100 kHz linewidth laser at 1550.1 nm was modulated at 28 GBaud using a IQ-modulator and pseudorandom binary sequences (PRBS) of length $2^{15} - 1$. The signal was then coupled into a recirculating loop using an acousto-optic modulator (AOM) where it was combined with a free-running high-power pump wave at 1554.1 nm and inserted into the FOPA acting as a copier with 14.2 dB net gain. The FOPA consisted of a cascade of four pieces of highly nonlinear fiber (HNLF) with isolators in between in order to suppress stimulated Brillouin scattering (SBS), more details on the FOPA implementation can be found in [16]. The generated idler wave was located at 1558.1 nm. The signal and idler waves were then separated from the pump in the launch power balancing stage where the launch powers of the signal and idler into the transmission span were balanced using a wavelength selective switch (WSS). After balancing, the launch powers were boosted by an EDFA and adjusted using a variable optical attenuator (VOA). When the link was operated in PIA mode, the idler wave was blocked by the WSS so that only the signal wave was transmitted. The pump wave was split up from the signal and idler balancing path and the pump launch power adjusted using a VOA. Since the pump recovery stage was based on injection locking, the pump wave was also transmitted alongside the

Optics EXPRESS

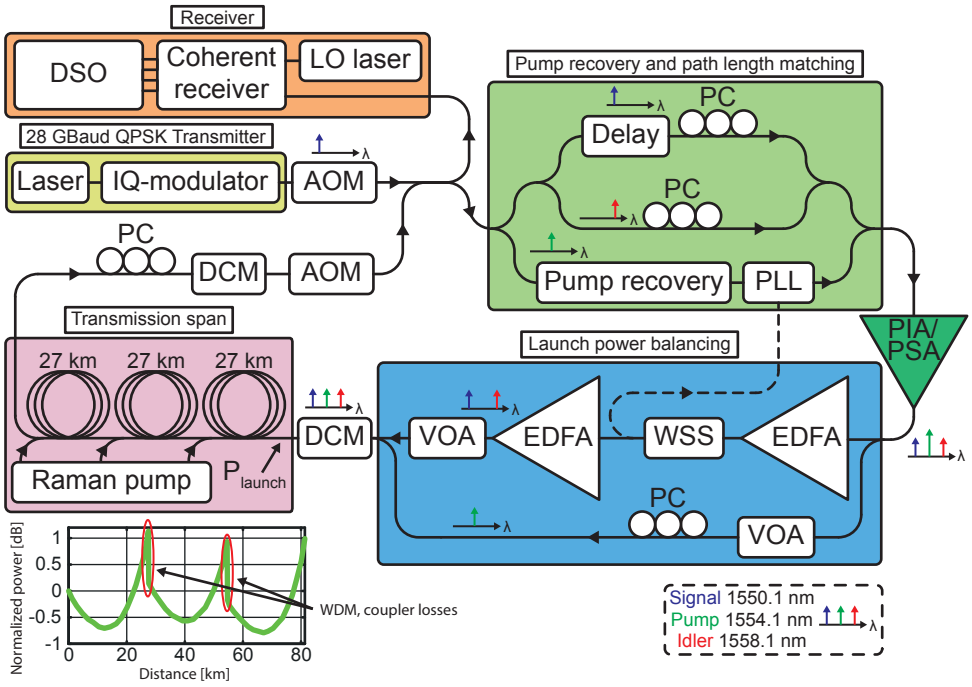

Fig. 1. Sketch of the experimental setup used to demonstrate hybrid PSA-DRA transmission. The same fiber-optic parametric amplifier (FOPA) acts as either PIA or PSA. The color coding used for illustrating the signal/idler/pump paths is shown in the bottom right. The results from an OTDR measurement of the span power map with DRA is shown in the bottom left.

signal and idler.

In order to achieve phase-sensitive amplification in the FOPA, the transmission span needs to be fully dispersion-compensated. This was achieved using tunable channelized fiber Bragg grating (FBG)-based dispersion compensating modules (DCMs) before and after the transmission span [17]. The ratio between dispersion pre- and post-compensation was optimized for each amplifier configuration in order to maximize the transmission reach in a nonlinear transmission regime. In order to achieve the flattest possible span power map with DRA, the span was divided into three 27 km segments that were individually backwards Raman pumped using a 1450 nm Raman fiber laser. In between each span segment was a wavelength division multiplexing (WDM) coupler for inserting the Raman pump as well as a monitor tap for measuring the signal launch power into each segment. The Raman pump powers into each segment were adjusted so that the signal launch power into each segment was the same, i.e. full transparency accounting for the losses of the WDM couplers and monitor taps in between each segment. A optical time-domain reflectometer (OTDR) operating at 1554 nm was used to measure the span power map with DRA. The results from these measurements are shown in the bottom left of Fig. 1 where we also note the impact of the WDM and coupler losses on the span power map. The loss of the segmented transmission span was 18 dB. It is clear that this implementation of DRA is not practical to use in real systems but we would like to point out that there are more practical DRA schemes that achieve similar levels of power map flatness without using remote optical pumping or placing active optical components inside each transmission span [18–21].

Before the FOPA on the second circulation the signal and idler waves were split up using a WDM coupler and path length matched so that they were synchronized into the FOPA on the

Optics EXPRESS

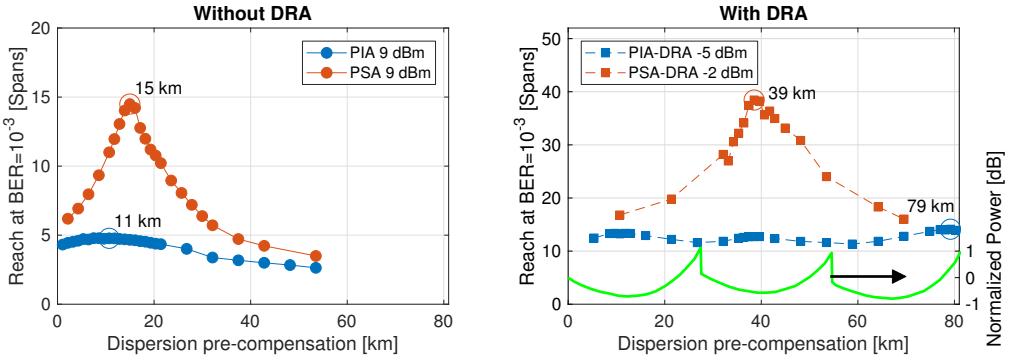

(a) (b)

Fig. 2. Optimization of the span dispersion map for the four different amplifier configurations. For each case, the optimum point has been encircled. (a) Transmission reach at BER = 10^{-3} as a function of dispersion pre-compensation for the PIA and PSA link. (b) Same for the PIA-DRA and PSA-DRA link. Referenced to the right axis is the measured span power map.

second passthrough. The pump recovery stage was based on an injection locked laser followed by a high-power EDFA and a phase-locked loop (PLL). The PLL operated by applying a 40 kHz phase dithering tone on the pump using a piezoelectric fiber stretcher and maximizing the PSA gain by keeping the relative phase between signal, idler and pump constant, more details on the PLL implementation can be found in [22]. Thus, the FOPA acted as a PSA on the second and all subsequent round trips in the loop. The PSA gain was 19.8 dB giving a gain difference of 5.6 dB when comparing PIA and PSA operation. The total loss between the point where launch power was measured and the PSA input was 36.6 dB.

After each circulation the signal was coupled out from the loop and detected using a coherent receiver with a free-running 100 kHz linewidth local oscillator (LO) laser at 1550.1 nm. The radio frequency (RF) signals from the coherent receivers balanced photodetectors were sampled using a 50 GS/s digital sampling oscilloscope (DSO) followed by offline DSP. The offline DSP consisted of dynamic equalization based on the constant modulus algorithm (CMA) using 141 T/2-spaced taps and phase tracking using the Viterbi-Viterbi algorithm followed by bit error rate (BER) counting. The large number of equalizer taps was needed because of the group delay ripple (GDR) in the DCMs. For each measurement point, ten 2.5 MSample batches were stored down for offline processing and the BER was found by averaging over the three best batches. This was done to reduce the impact of the batches where e.g. the injection locking or the PLL failed at many roundtrips.

3. Experimental results

The experimental results are presented in two parts. First, we present results from the optimization of the span dispersion map for the different amplifier configurations. Second, the optimal span dispersion maps found will be used in long haul transmission to estimate the transmission reach.

3.1. Dispersion map optimization

The dispersion map was swept by changing the ratio between dispersion pre- and post-compensation. The fact that we used tunable DCMs for dispersion compensation enabled this sweep to be performed experimentally. The residual dispersion was set to zero for all cases.

Optics EXPRESS

For each of the amplifier configurations, the transmission reach at BER = 10^{-3} was measured with different dispersion maps at a launch power approximately 3 dB above optimal launch power. This choice was made in order to enhance the nonlinear distortion, making it easier to distinguish the optimum point. Note that the differences in reach for different dispersion maps is dictated by nonlinear distortion, i.e. in a linear transmission regime the dispersion map does not impact performance. The results from these measurements are presented in Fig. 2 where the transmission distance at BER = 10^{-3} is shown as a function of the dispersion pre-compensation for the four different amplifier configurations. The dispersion map sweeps for the PIA and PSA links are shown in Fig. 2(a) and for the PIA-DRA and PSA-DRA links in Fig. 2(b). In the cases without DRA we see that the dispersion pre-compensation optimum shifts from 11 km to 15 km when enabling phase-sensitive amplification by transmission of both signal and idler waves. For the cases with DRA, the difference between the characteristics of the PIA and PSA curve is more pronounced and the optimum shifts from 79 km to 39 km when enabling phase-sensitive amplification. The ripple behavior observed in the PIA-DRA case is due to the three individually Raman pumped span segments causing a periodic power map within one transmission span.

On the one hand, the fact that we observe sharp peaks in the PSA and PSA-DRA cases shows that the PSAs are in fact compensating for the nonlinear phase shift. On the other hand, the sharp optima could pose an issue in practical systems due to the required precision of the ratio between dispersion pre- and post-compensation.

3.2. *Long-haul transmission*

Using the optimal dispersion maps, a launch power sweep was performed, measuring the transmission reach at BER = 10^{-3} for different signal launch powers. In Figs. 3(a) and 3(b), the transmission reach is shown as a function of signal launch power for the four amplifier configurations. The launch power is defined as the optical power of the signal wave only, not taking into account the power of the idler wave. The transmission reach as a function of signal launch power for the PIA and PSA link is shown in Fig. 3(a). We see that the optimal launch power is 6 dBm for the PIA case and 5 dBm for the PSA case. The transmission reach is approximately 6 roundtrips for the PIA link and 23 roundtrips for the PSA link. This gives a transmission reach increase by a factor of 3.8 when comparing the PSA link to the PIA link and a total accumulated nonlinear phase shift of 2.0 radians for the PSA link at 23 roundtrips and 5 dBm launch power. The total accumulated nonlinear phase shift of the PIA link at 6 round trips and 6 dBm launch power was 0.7 radians. The transmission reach as a function of signal launch power for the PIA and PSA link with DRA is shown in Fig. 3(b). We see that the optimal launch power of the PIA link with DRA is -8 dBm while the PSA link with DRA has an optimal launch power of -6 dBm. The transmission reach for the PIA-DRA case is 15 roundtrips and 44 roundtrips for the PSA-DRA case. The total accumulated nonlinear phase shift for the PSA-DRA link at 44 roundtrips and -6 dBm launch power was 1.1 radians. The total accumulated nonlinear phase shift of the PIA-DRA link at 15 round trips and -8 dBm launch power was 0.2 radians. In Figs. 3(c) and (d) we show the reach increase factor as a function of launch power when comparing PIA to PSA and PIA-DRA to PSA-DRA, respectively. We note that for the cases without DRA that the reach increase factor decreases when the launch power is increased while the opposite is true for the cases with DRA. In the DRA cases the reach increase factor improves significantly when moving beyond optimal launch power. At very high launch powers the reach increase factors even exceed above the 4x factor that is expected [13] in a linear transmission regime dominated by ASE from the FOPA.

4. Numerical analysis

Simulations were performed to estimate the performance of the PSA-DRA link in Fig. 1 and compare to experimental results. In the simulations, a signal and idler wave modulated with 28 GBaud QPSK was propagated using independent split-step Fourier method (SSFM) solvers taking

Optics EXPRESS

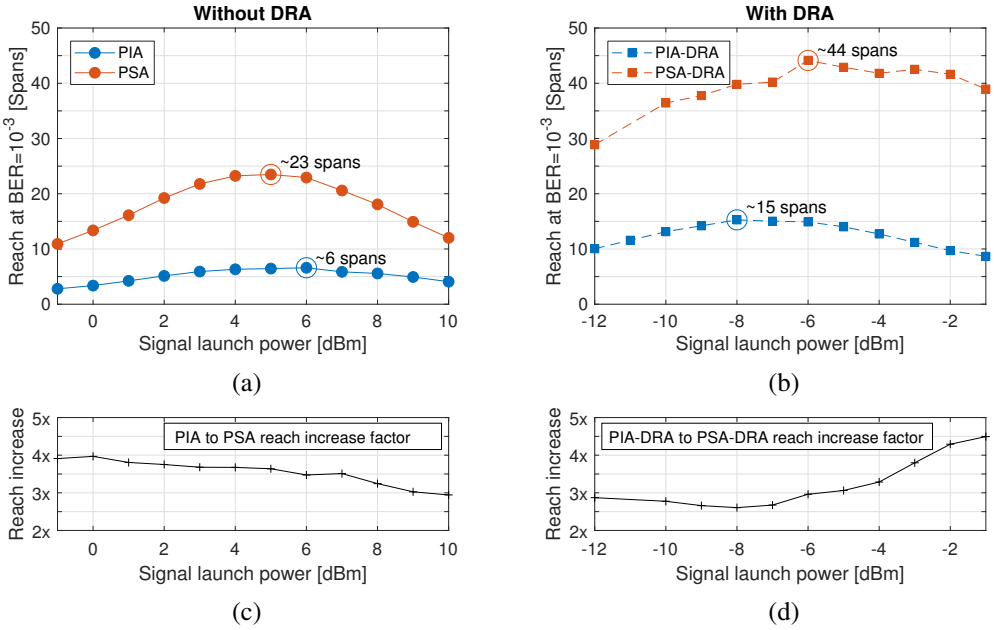

Fig. 3. Transmission reaches and reach increase factors as a function of signal launch power. For each case the point with the longest transmission reach have been encircled. (a) Reach at BER = 10^{-3} as a function of signal launch power for the PIA and PSA link. (b) Reach at BER = 10^{-3} as a function of signal launch power for the PIA-DRA and PSA-DRA link. (c) Reach increase factor when going from PIA to PSA as a function of launch power. (d) Reach increase factor when going from PIA-DRA to PSA-DRA as a function of launch power.

into account backwards Raman pumping in the segmented span. Noise from DRA was added in each split-step. The segmented span was modeled with a 1 dB lumped loss in between each segment giving a span power map similar to the measurement shown in Fig. 1. The Raman pump power was set so that each span segment was transparent accounting for the loss between segments. The excess loss of 18.6 dB after the transmission span due to dispersion post-compensation, loop components and the path length matching stage was also taken into account. The PSA noise figure was set to 1.4 dB. The amount of dispersion pre- and post-compensation was optimized for the PSA-DRA case and the optimal dispersion map used to simulate long haul transmission. The PSA after each span was modeled using a simplified matrix formulation in the same way as described in [14]. The same receiver DSP as in the experiments was used to process the received waveforms. The fiber parameters were L_{span} = 80 km, α_{signal} = 0.2 dB/km, $\alpha_{\text{Raman pump}}$ = 0.25 dB/km, D = 17 ps nm^{-1}km^{-1}, γ = 1.3 W^{-1}km^{-1}. In order to investigate the penalty from the FBG-based DCMs we made simulations both with and without taking the GDR and passband characteristic of the DCMs into account. The amplitude response and GDR of the simulated DCMs are shown in Fig. 4(b). Since the signal passed through the same two DCMs repeatedly in the recirculating loop experiment, the GDR was modelled by adding up the GDR of two passbands. This was done independently for the signal and idler, i.e. the signal experienced the summation of the ripple labeled signal phase A and B in Fig. 4(b) and the idler experiences the summation of idler phase A and B. It should however be noted that the GDR ripple used in simulations were not from the exact same units that were used in the experiments. Statistical fluctuations in GDR between specific units will cause differences in performance, this was however not studied. The results

Optics EXPRESS

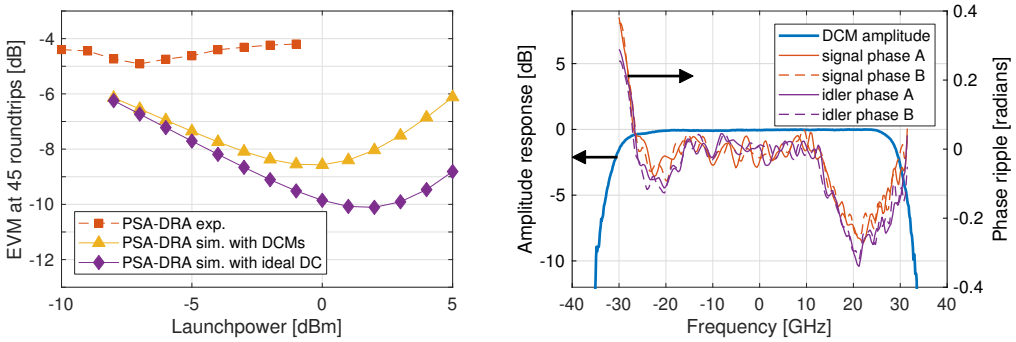

(a) (b)

Fig. 4. Results from the simulations in comparison to experimental results. (a) The EVM at 45 roundtrips as a function of launch power for three cases, experimental, simulated with realistic modelling of the DCMs and simulated with ideal dispersion compensation. (b) The amplitude and phase responses of the simulated DCMs.

from the simulations are presented in Fig. 4(a) where the error vector magnitude (EVM) is shown as a function of launch power at 45 roundtrips and compared to the experimental results. As one might expect, the passband characteristics and GDR of the DCMs imposes a EVM penalty on the nonlinearity mitigation, reducing the optimal launch power in simulations by 2-3 dB. However it is also clear that the penalties from the GDR and passband characteristics of the DCMs is not sufficient to explain the experimental results fully since the optimum launch power in the experiments was 6 dB lower than in the simulations with DCMs. A longer discussion on this will follow in Section 5.

5. Discussion

In order for the PSAs to compensate nonlinear distortion efficiently it is important to chose a proper span dispersion map. We performed this optimization experimentally using tunable DCMs. The results from these measurements were shown in Fig. 2. When we studied the dispersion map sweep results for the PSA-DRA case, we observed a peak centered around 39 km. This is close to the 50 % dispersion pre-compensation predicted for the case with a perfectly flat or symmetric span power map [14]. Considering the shift in the optimum dispersion map between the PIA-DRA case and the PSA-DRA case, this indicates that the nonlinearity compensation through coherent superposition in the PSAs is working and that this effect is dominating over other interactions between dispersive and nonlinear effects.

Another important issue to discuss is the impact of DRA on the equivalent span NF. Assuming the span and excess losses measured in the experiment, ideal DRA, a 1 dB PSA NF and a 4 dB PIA NF one can obtain simple analytical estimates of the linear span NF for each of the different amplifier configurations. The equivalent span NF of a 81 km span with ideal DRA is 9.3 dB. The equivalent span NF for the four different amplifier configurations can be found using Friis formula. The equivalent span NF for the PIA case is 40.6 dB, for the PSA case 37.6 dB, for the PIA-DRA case 22.8 dB and for the PSA-DRA case 19.9 dB. This tells us that even in the cases with DRA the signal-to-noise ratio (SNR) degradation from the FOPA is larger than that from the DRA. Using the numerical simulations presented in Section 4 it was estimated that the nonlinear phase shift at a given launch power was increased by 5.7 dB when turning on the DRA.

Examining the launch power sweeps presented in Fig. 3 we need to discuss a few important

Optics EXPRESS

features. First of all we note that for the cases without DRA, the optimal launch power stays essentially unchanged when comparing the PIA and PSA case. If we instead look at the cases with DRA we note that the optimal launch power is increased by 2 dB when going from PIA-DRA to PSA-DRA. We interpret this as mainly being due to improved nonlinearity mitigation even though it is important to note that the difference in equivalent span NF between the PIA and PSA case will affect the optimum launch power difference between the two cases. Second, we discuss the transmission reach in the PSA-DRA case. When comparing experiments to simulations it becomes clear that the transmission reach in the PSA-DRA is shorter than what is predicted by the simulations. More importantly it is clear that the optimal launch power is lower in the experiments than in simulations by a margin of approximately 6 dB. This leads us to believe that there are significant penalties impacting the efficiency of the nonlinearity mitigation due to various nonidealities beyond our control in the presented experiment. One important feature of the experiment is that we are using channelized tunable DCMs based on FBG technology [17]. The advantage of using these is that we can perform the dispersion map optimization experimentally and do not need to rely on numerical simulations for finding the optimal dispersion map. The disadvantage is that the DCMs have a limited optical bandwidth and group delay ripple. It is reasonable to believe that the GDR will cause penalties both in terms of the signal and idler waves into the PSA not fulfilling phase-matching conditions as well as reducing the efficiency of the nonlinearity mitigation. Both the GDR and passband characteristic penalties are made worse by the fact that we propagate through the same DCMs in every roundtrip. This causes the group delay ripple to accumulate in a correlated manner as we pass through the DCMs repeatedly. It was also confirmed in the simulations that there is a significant penalty due to the DCM characteristics.

Other reasons for having a significant penalty compared to the simulations is that we use injection locking and noise accumulates on the pump as we propagate. We also have non-idealities regarding the span power map symmetry between signal and idler which will reduce the efficiency of the nonlinearity mitigation. Since we are using a single backwards Raman pump, the gain spectrum of the DRA is not perfectly flat over the 8 nm spanned by the signal and idler wave. This will cause penalties relative to the ideal scenario in the simulations where it was assumed that the signal and idler propagate with the same span power map. Another effect that was not taken into account in the simulations was double Rayleigh backscattering which will cause an effective SNR degradation at high launch powers in spans with transparency or high DRA gain [23]. The effects of polarization mode dispersion (PMD) and third-order dispersion were also neglected in the numerical modelling as well as XPM from signal and idler onto the co-propagating pump wave.

6. Conclusion

We have for the first time demonstrated long-haul transmission with a hybrid amplifier approach combining the copier-PSA scheme with DRA. This hybrid amplifier approach was implemented in a recirculating loop experiment to examine the nonlinearity mitigation properties of the PSAs and to investigate whether it was possible to improve the PSA nonlinearity compensation with the addition of DRA. For the study we performed measurements using four different amplifier configurations, PIA, PSA, hybrid PIA-DRA and hybrid PSA-DRA. By looking solely at the increase in transmission reach when comparing the PSA case to the PSA-DRA case it was not possible to draw the conclusion that the nonlinearity compensation was improved since the total accumulated nonlinear phase shift at a distance corresponding to e.g. BER = 10^{-3} at optimal launch power was lower in the PSA-DRA case (1.1 radians) compared to the PSA case (2.0 radians). This can be explained by penalties at long distances as well as nonidealities reducing the efficiency of the nonlinearity mitigation. We believe that an important contributing factor to these penalties was nonidealities in the inline dispersion compensation and this was also confirmed in simulations. A 2 dB increase in optimal launch power was, however, observed when comparing the PIA-DRA case to the PSA-DRA case, indicating improved nonlinearity compensation. When

Optics EXPRESS

going from PIA to PSA, the transmission reach increase factor at optimal launch powers was 3.8 while from PIA-DRA to PSA-DRA, the reach improved by a factor of 2.9.

Funding

Swedish Research Council (VR) (2015-00535)

Acknowledgments

The authors would like to acknowledge Attila Fülöp and Mikael Mazur for useful advice regarding the experimental setup and assistance with the receiver DSP. Egon Astra is acknowledging support from the Study IT in Estonia programme. The authors would like to thank OFS Denmark for providing HNLFs. The simulations were performed on resources at Chalmers Centre for Computational Science and Engineering (C3SE) provided by the Swedish National Infrastructure for Computing (SNIC).

129.16.88.140 (fo 2018-08-14 04:28:51)